Table 1
Patient characteristics

Variable	Total (n=17)	AF (n=7)	Sinus rhythm (n=10)
Age (yrs)	59 ± 16	64 ± 9	56 ± 18
Left atrial diameter (mm)	52 ± 15	67 ± 9*	42 ± 7
LV ejection fraction (%)	60 ± 13	62 ± 13	58 ± 14
MR grade	2.2 ± 1.4	2.7 ± 1.0	1.8 ± 1.0
TR grade	2.0 ± 1.4	2.7 ± 1.0	1.5 ± 1.0
Systolic PA pressure (mmHg)	39.9 ± 14.0	45.0 ± 14.0	35.4 ± 14.0
Mean RA pressure (mmHg)	6.5 ± 3.5	8.6 ± 4.0	4.8 ± 1.0
Digitalis (n)	9	7	2
Systolic blood pressure (mmHg)	133 ± 25	134 ± 26	133 ± 25
Diastolic blood pressure (mmHg)	71 ± 16	75 ± 20	69 ± 13
Fasting blood sugar (mg/dl)	101 ± 15	90 ± 7†	107 ± 15
Total cholesterol (mg/dl)	195 ± 44	208 ± 41	189 ± 46
Triglyceride (mg/dl)	123 ± 64	118 ± 54	125 ± 71

Data are mean ±S.D. or n. *P<0.001 and †P<0.02 compared with sinus rhythm patients. AF, atrial fibrillation; LV, left ventricular; MR, mitral valve regurgitation; PA, pulmonary arterial; RA, right atrial; TR, tricuspid valve regurgitation.

using multiple cDNA or oligonucleotide samples placed on a glass slide, investigators can analyze several thousand full-length genes or expressed oligonucleotide sequences at once. In addition to identifying large clusters of genes that respond to a given stimulus, DNA microarray technology may be used to identify some genes that comprise highly specific molecular responses [5,6]. Already, some studies using microarray technology have yielded interesting results regarding the pathogenesis of cardiovascular diseases, such as myocardial infarction [7], cardiac hypertrophy [8], and human heart failure [9]. In the present study, we used DNA microarray technology to investigate the transcriptional profiling of genes modulated in the right atrium of patients with AF compared with sinus rhythm.

2. Methods

2.1. Subjects

This study group consisted of seven patients with AF (mean age 64±9 years) and 10 patients with sinus rhythm (mean age 56±18 years) who underwent cardiac surgery (Table 1). The underlying heart diseases in the patients are shown in Table 2. Hemodynamic studies were performed the morning after an overnight fast. Vasodilators were withheld for at least 24 h before evaluation. Chronic, stable doses of digoxin, and diuretics were continued but were administered on an evening schedule. Right and left heart studies, including measurement of pressure, biplane left ventriculography and coronary angiography, were performed using a percutaneous cathether. Left ventricular ejection fraction was determined by the area-length method [10]. The severity of mitral regurgitation was assessed according to the method of Sellers et al. [11]. Transthoracic echocardiography was performed in all patients using a Hewlett-Packard SONOS 5500 system (Hewlett-Packard, Palo Alto, CA) with a 2.5 MHz transducer. The left atrial diameter was determined by M-mode echocardiography [12]. The severity of tricuspid regurgitation was graded on a four-point scale, based on the distance reached by the abnormal signals from the tricuspid orifice toward the posterior wall in the parasternal four-chamber view [13].

This study was approved by our institutional human investigations committee, and written informed consent was obtained from all patients before participation.

2.2. Atrial myocardium samples

Right atrial appendages were obtained from the patients during cardiac surgery. Pieces of right atrial appendage weighing 200–1400 mg were frozen immediately in liquid nitrogen, and stored at −80 °C.

Table 2
Underlying heart disease

Patients	Age	Sex	Diagnosis
Sinus group			
1	44	M	AR
2	70	F	MR
3	75	M	AP
4	65	M	AS
5	60	M	AS
6	64	F	MR
7	64	F	AR, MR
8	15	M	ASD
9	63	M	AR
10	36	F	ASD
AF group			
1	51	F	MS
2	55	M	MR
3	64	M	MR
4	74	F	ASR, MSR
5	75	M	ASR, MR
6	59	F	MS
7	69	F	MSR

AP, angina pectoris; AR, aortic valve regurgitation; AS, aortic valve stenosis; ASD, atrial septal defect; ASR, aortic valve stenosis and regurgitation; MR, mitral valve regurgitation; MS, mitral valve stenosis; MSR, mitral valve stenosis and regurgitation.

2.3. Transcriptional profiling

A DNA microarray was used for each specimen. Total RNA was extracted using RNAzol B (TEL-TEST, Friendswood, TX), and the purity was checked by spectrophotometry and agarose gel electrophoresis. Total RNA (5 μg) was converted to double-stranded cDNA using an oligo dT primer containing the T7 promoter (Gibco BRL Superscript® Choice System; Life Technologies, Rockville, MD), and the template for an in vitro transcription reaction was used to synthesize biotin-labeled antisense cRNA (Bio-Array™ High Yield RNA Transcript Labeling Kit; Enzo Diagnostics, Farmingdale, NY). The biotinylated cRNA was fragmented and hybridized for 16 h at 45 °C to GeneChip Test2 arrays (Affymetrix, Santa Clara, CA) to assess sample quality, and then to Human Genome arrays (U95A, Affymetrix). The arrays were washed, and then stained with streptavidin-phycoerythrin. The arrays were scanned with the GeneArray scanner (Agilent Technologies, Palo Alto, CA) and analyzed using the GeneSpring software package (Silicon Genetics, Redwood City, CA). Human Genome U95A was derived from GenBank 113 and dbEST/10-02-99.

Detailed protocols for data analysis of Affymetrix oligonucleotide microarrays and extensive documentation of the sensitivity and quantitative aspects of the method have been described [14–16]. Briefly, each gene is represented by the use of ~20 perfectly matched (PM) and mismatched (MM) control probes. The MM probes act as specificity controls that allow the direct subtraction of both background and cross-hybridization signals. The number of instances in which the PM hybridization signal is larger than the MM signal is computed along with the average of the logarithm of the PM:MM ratio (after background subtraction) for each probe set. These values are used to make a matrix-based decision concerning the presence or absence of an RNA molecule. Positive average signal intensities after background subtraction were observed for over 12,000 genes for all samples. To determine the quantitative RNA abundance, the average of the differences representing PM minus MM for each gene-specific probe family is calculated, after discarding the maximum, the minimum, and any outliers beyond 3 SDs.

2.4. Real-time reverse transcription (RT)-PCR analysis

For reverse transcription (RT), RNA obtained from each specimen was reverse transcribed using T7-dT primer (5′-TCT AGT CGA CGG CCA GTG AAT TGT AAT ACG ACT CAC TAT AGG GCG TTT TTT TTT TTT TTT TTT TTT-3′) and Superscript II reverse transcriptase (Life Technologies). Real-time quantitative PCR was performed in optical tubes in a 96-well microtiter plate (Perkin-Elmer/Applied Biosystems, Foster City, CA) with an ABI PRISM 7700 Sequence Detector Systems (Perkin-Elmer/Applied Biosystems) according to the manufacturer's instructions. By using the SYBR Green PCR Core Reagents Kit (Perkin-Elmer/Applied Biosystems, P/N 4304886), fluorescence signals were generated during each PCR cycle via the 5′-to 3′-endonuclease activity of Taq Gold [17] to provide real-time quantitative PCR information. The oligonucleotide primers used for real-time PCR analysis are shown in Table 3. No template controls as well as the samples were added in a total volume of 50 μl/reaction. Potential PCR product contamination was digested by uracil-*N*-glycosylase, because dTTP is substituted by dUTP [17]. All PCR experiments were performed with the hot start method. In the reaction system, uracil-*N*-glycosylase and Taq Gold (Perkin-Elmer/Applied Biosystems) were applied according to the manufacturer's instructions [17,18]. Denaturing and annealing reactions were performed 40 times at 95 °C for 15 s, and at 60 °C for sarcoplasmic reticulum Ca^{2+}-ATPase 2, 66 °C for nuclear factor-interleukin 6 (NF-IL6)-beta and 62 °C for glyceraldehyde-3 phosphate dehydrogenase (GAPDH) for 1 min, respectively. The increase in the fluorescence signal is proportional to the amount of specific product [14]. The intensity of emission signals in each sample was normalized to that of GAPDH as an internal control.

2.5. Statistical analysis

Raw data from array scans were averaged across all gene probes for each array, and a scaling factor was applied to bring the average intensity for all probes on the array to 2500. This allows any sample to be normalized for comparison with any other comparable sample.

Table 3
Primer design for real-time PCR analysis

Gene		Primer sequence	PCR product size (bp)
NF-IL6-beta	Sense	5′-CACAGACCGTGGTGAGCTTG-3′	257
	Antisense	5′-CACCAACTTCTGCTGCATCTC-3′	
Sarcoplasmic reticulum	Sense	5′-TTTCTGGTACAAACATTGCTGC-3′	140
Ca^{2+}-ATPase 2	Antisense	5′-TAGTTTTTGCTGAAGGGGTGTT-3′	
GAPDH	Sense	5′-CTTTGGTATCGTGGAAGGACTC-3′	140
	Antisense	5′-CAGTAGAGGCAGGGATGATGTT-3′	

GAPDH, glyceraldehyde-3 phosphate dehydrogenase; NF-IL6, nuclear factor-interleukin 6.

Table 4
Analysis of AF-specific genes by DNA microarray

Function	Gene	Fold change	Genbank#
Antioxidants	Glutathione peroxidase	1.8 ± 1.1	X13710
Cell growth	Vascular endothelial growth factor B	1.6 ± 0.7	U43368
Cell signaling	RhoC	1.6 ± 0.5	L25081
Inflammation	Macrophage migration inhibitory factor	1.7 ± 0.6	L19686
Proto-oncogene	A-raf-1 oncogene	1.5 ± 0.5	U01337
Transcription	NF-IL6-beta	2.0 ± 0.7	M83667

Data are mean ±S.D. Fold change was relative to sinus rhythm group. NF-IL6, nuclear factor-interleukin 6.

Data are expressed as the mean ± S.D. Differences were analyzed with the Mann–Whitney *U* test for unpaired observations. A *P*-value of <0.05 was considered significant.

3. Results

3.1. Patient characteristics

As shown in Table 1, the left atrial diameter in the AF group was significantly greater than that in the sinus rhythm group ($P<0.001$). In addition, the levels of fasting blood sugar in the AF group were significantly lower than those in the sinus rhythm group ($P<0.02$). There were no other differences detected between the sinus rhythm group and AF group.

3.2. DNA microarray analysis of AF-specific genes

We identified 33 AF-specific genes that were significantly activated (>1.5-fold, $P<0.05$), compared with those in the sinus rhythm group, including an ion channel, an antioxidant, an inflammation, three cell growth/cell cycle, three transcription, several cell signaling and several protein genes, and seven expressed sequence tags (ESTs). Some of the selected genes are shown in Table 4. All data are available in an online only Data Supplement at http://www.elsevier.com/locate/inca/506041.

3.3. DNA microarray analysis of sinus rhythm-specific genes

In contrast, we found 63 sinus rhythm-specific genes, including several cell signaling/communication genes such as sarcoplasmic reticulum Ca^{2+}-ATPase 2, several cellular respiration and energy production and two antiproliferative or negative regulator of cell growth genes, and 22 ESTs (<0.5-fold, $P<0.05$). Some of the selected genes are shown in Table 5. All data are available in an online only Data Supplement at http://www.elsevier.com/locate/inca/506041.

3.4. Real-time RT-PCR analysis

We focused on two of the genes screened by the oligonucleotide microarray: NF-IL6-beta and sarcoplasmic reticulum Ca^{2+}-ATPase 2. NF-IL6-beta is an important transcriptional activator in the regulation of genes involved in the immune and inflammatory response [19]. AF may persist due to structural changes in the atria that are promoted by inflammation [20]. In addition, cytosolic Ca^{2+} overload may be an important mediator of AF. Abnormalities in the Ca^{2+} regulatory proteins, such as sarcoplasmic reticulum Ca^{2+}-ATPase 2, of the atrial myocardium in chronic AF patients may be involved in the initiation and/or perpetuation of AF. These genes were confirmed by the real-time RT-PCR method. As shown in Fig. 1, NF-IL6-beta mRNA expression in the AF group was significantly higher than that in the sinus rhythm group ($P<0.02$). In contrast, as shown in Fig. 2, sarcoplasmic reticulum Ca^{2+}-ATPase 2 mRNA expression in the AF group was lower compared with that in the sinus rhythm group ($P<0.1$), but not significantly.

4. Discussion

The cellular and molecular basis of AF has been a field of enormous interest over the past few years. However, the

Table 5
Analysis of sinus rhythm-specific genes by DNA microarray

Function	Gene	Fold change	Genbank#
Antioxidants	Peroxiredoxin 3	0.5 ± 0.2	D49396
Cell signaling	Caveolin 2	0.4 ± 0.3	AF035752
Cell signaling	Sarcoplasmic reticulum Ca^{2+}-ATPase 2	0.4 ± 0.3	M23115
Cell signaling	Connexin 43	0.4 ± 0.3	X52947
Proto-oncogene	Ras-associated protein rab1	0.5 ± 0.2	AL050268

Data are mean ±S.D. Fold change was relative to sinus rhythm group.

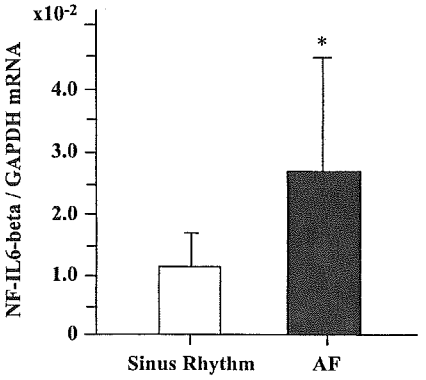

Fig. 1. Nuclear factor-interleukin 6 (NF-IL6)-beta mRNA expression in the right atria of patients with sinus rhythm and atrial fibrillation (AF). Total RNA obtained from the right atria of patients with sinus rhythm (n=10) and AF (n=7) using RNAzol B (TEL-TEST) was analyzed by quantitative real-time reverse transcription-PCR as described in Methods. The amount of mRNA expression for NF-IL6-beta was standardized to that of glyceraldehyde-3 phosphate dehydrogenase (GAPDH) mRNA expression. Data are means±S.D. *P<0.02 compared with sinus rhythm patients.

mechanism of AF in human tissues is extremely complex, because atrial remodeling consists of electrical, contractile, and structural remodeling. In addition, structural remodeling may occur from chronic hemodynamic, metabolic, or inflammatory stressors. Many factors such as ion channels, proteins influencing calcium homeostasis, connexins, autonomic innervation, fibrosis, paracrine factors, and cytokines may be involved in the molecular mechanism of AF. The present study using oligonucleotide microarray analysis demonstrated that about one hundred genes were modulated in the right atrium of patients with AF. These findings suggest that these genes may play critical roles in the initiation or perpetuation of AF and the pathophysiology of atrial remodeling.

In the present study, DNA microarray analysis identified 33 AF-specific genes. Some of these genes encode NF-IL6-beta, macrophage migration inhibitory factor, A-raf-1 oncogene, vascular endothelial growth factor B, RhoC, and glutathione peroxidase. NF-IL6-beta mRNA expression induced in the atria of AF patients was confirmed by the real-time PCR method. NF-IL6-beta and macrophage migration inhibitory factor are involved in inflammation [19,21]. Chung et al. [20] reported that C-reactive protein, a marker of systemic inflammation, is elevated in AF patients compared with sinus rhythm patients. Novel and inflammatory mechanisms may promote the persistence of AF, potentially by inducing structural and/or electrical remodeling of the atria. A-raf-1 protooncogene encodes cytoplasmic protein serine/threonine kinase, which plays an important role in cell growth and development [22]. Vascular endothelial growth factor B with structural similarities to vascular endothelial growth factor and placenta growth factor has a role in angiogenesis and endothelial cell growth [23]. RhoC, small guanosine triphosphatase Rho, which regulates remodeling of the actin cytoskeleton during cell morphogenesis and motility [24], may contribute to the structural remodeling. Baumer et al. [25] demonstrated that the activity, mRNA, and protein levels of glutathione peroxidase, an antioxidative enzyme, decreased in human failing myocardium. However, the present study showed that the glutathione peroxidase mRNA level in AF patients was elevated.

The present study demonstrated that the expression of 63 genes in AF patients was significantly lower compared with sinus rhythm. For example, genes for sarcoplasmic reticulum Ca^{2+}ATPase 2 and connexin 43 in AF patients were downregulated. In the real-time PCR analysis, sarcoplasmic reticulum Ca^{2+}-ATPase 2 mRNA expression in the AF group was lower compared with that in the sinus rhythm group, but not significantly. Ohkusa et al. [26] also reported that sarcoplasmic reticulum Ca^{2+}-ATPase 2 mRNA in both the right and left atrial myocardial tissues from 13 patients with AF were significantly lower than in the right atrium of patients with sinus rhythm. A decrease in sarcoplasmic reticulum Ca^{2+}-ATPase 2 in the atria may sustain abnormal intracellular Ca^{2+} handling and changes in the electrophysiologic properties of atrial tissue, leading to the perpetuation of AF. Connexin 43 is one of the gap junctions that are clusters of closely packed channels. Gap junctions directly connect the cytoplasmic compartments of neighboring cells and allow the passage of ions and small molecules. In the present study, connexin 43 mRNA expression in AF patients was downregulated. It is still controversial whether connexin 43 is upregulated [27], unchanged or downregulated in AF. Thus, changes in the expressions of connexin 43 might affect conduction velocity, contributing to sustained AF.

Previous studies demonstrated that some genes including L-type calcium channel [28], potassium channels [29], and sarcoplasmic reticulum Ca^{2+}-ATPase 2 [26,28] are modulated in AF patients. However, the molecular

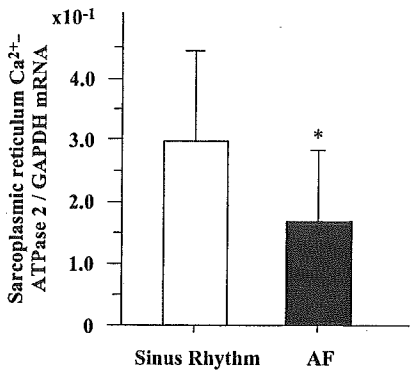

Fig. 2. Sarcoplasmic reticulum Ca^{2+}-ATPase 2 mRNA expression in the right atria of patients with sinus rhythm and atrial fibrillation (AF). Total RNA obtained from the right atria of patients with sinus rhythm (n=10) and AF (n=7) using RNAzol B (TEL-TEST) was analyzed by quantitative real-time reverse transcription-PCR as described in Methods. The amount of mRNA expression for sarcoplasmic reticulum Ca^{2+}-ATPase 2 was standardized to that of glyceraldehyde-3 phosphate dehydrogenase (GAPDH) mRNA expression. Data are means±S.D. *P<0.1 compared with sinus rhythm patients.

mechanism of AF is poorly understood. Although the roles of other genes including ESTs in the heart except for the genes described above still remain unknown, the genes screened in this study may provide insights into the initiation or perpetuation of AF and the pathophysiology of atrial remodeling, because DNA microarray is a highly effective method for screening genes.

Acknowledgements

This study was supported by grants from the Ministry of Education, Science, Sports and Culture of Japan (15590769), Tokyo, Japan, the Mitsui Life Social Welfare Foundation, Tokyo, Japan, the Takeda Science Foundation, Osaka, Japan, the Daiwa Securities Health Foundation, Tokyo, Japan, and the Sankyo Foundation of Life Science, Tokyo, Japan.

References

[1] Cerebral Embolism Task Force. Cardiogenic brain embolism. Arch Neurol 1986;43:71–84.
[2] Wolf PA, Dawber TR, Thomas Jr HE, Kannel WB. Epidemiologic assessment of chronic atrial fibrillation and risk of stroke: the Framingham study. Neurology 1978;28:973–7.
[3] Okishige K, Sasano T, Yano K, Azegami K, Suzuki K, Itoh K. Serious arrhythmias in patients with apical hypertrophic cardiomyopathy. Intern Med 2001;40:396–402.
[4] Redfield MM, Kay GN, Jenkins LS, Mianulli M, Jensen DN, Ellenbogen KA. Tachycardia-related cardiomyopathy: a common cause of ventricular dysfunction in patients with atrial fibrillation referred for atrioventricular ablation. Mayo Clin Proc 2000;75:790–5.
[5] Iyer VR, Eisen MB, Ross DT, et al. The transcriptional program in the response of human fibroblasts to serum. Science 1999;283:83–7.
[6] Feng Y, Yang JH, Huang H, et al. Transcriptional profile of mechanically induced genes in human vascular smooth muscle cells. Circ Res 1999;85:1118–23.
[7] Stanton LW, Garrard LJ, Damm D, et al. Altered patterns of gene expression in response to myocardial infarction. Circ Res 2000;86:939–45.
[8] Friddle CJ, Koga T, Rubin EM, Bristow J. Expression profiling reveals distinct sets of genes altered during induction and regression of cardiac hypertrophy. Proc Natl Acad Sci U S A 2000;97:6745–50.
[9] Yang J, Moravec CS, Sussman MA, et al. Decreased SLIM1 expression and increased gelsolin expression in failing human hearts measured by high-density oligonucleotide arrays. Circulation 2000;102:3046–52.
[10] Greene DG, Carlisle R, Grant C, Bunnell IL. Estimation of left ventricular volume by one-plane cineangiography. Circulation 1967;35:61–9.
[11] Sellers RD, Levy MJ, Amplatz K, Lillehei CW. Left retrograde cardioangiography in acquired cardiac disease: technic, indications and interpretation in 700 cases. Am J Cardiol 1964;14:437–47.
[12] Sahn DJ, DeMaria A, Kisslo J, Weyman A. Recommendations regarding quantitation in M-mode echocardiography: results of a survey of echocardiographic measurements. Circulation 1978;58: 1072–1083.
[13] Miyatake K, Okamoto M, Kinoshita N, et al. Evaluation of tricuspid regurgitation by pulsed Doppler and two-dimensional echocardiography. Circulation 1982;66:777–89.
[14] Lockhart DJ, Dong H, Byrne MC, et al. Expression monitoring by hybridization to high-density oligonucleotide arrays. Nat Biotechnol 1996;14:1675–80.
[15] Lee CK, Klopp RG, Weindruch R, Prolla TA. Gene expression profile of aging and its retardation by caloric restriction. Science 1999; 285:1390–3.
[16] Golub TR, Slonim DK, Tamayo P, et al. Molecular classification of cancer: class discovery and class prediction by gene expression monitoring. Science 1999;286:531–7.
[17] Heid CA, Stevens J, Livak KJ, Williams PM. Real time quantitative PCR. Genome Res 1996;6:986–94.
[18] Kruse N, Pette M, Toyka K, Rieckmann P. Quantification of cytokine mRNA expression by RT PCR in samples of previously frozen blood. J Immunol Methods 1997;210:195–203.
[19] Kinoshita S, Akira S, Kishimoto T. A member of the C/EBP family, NF-IL6 beta, forms a heterodimer and transcriptionally synergizes with NF-IL6. Proc Natl Acad Sci U S A 1992;89:1473–6.
[20] Chung MK, Martin DO, Sprecher D, et al. C-reactive protein elevation in patients with atrial arrhythmias: inflammatory mechanisms and persistence of atrial fibrillation. Circulation 2001;104:2886–91.
[21] Bacher M, Metz CN, Calandra T, et al. An essential regulatory role for macrophage migration inhibitory factor in T-cell activation. Proc Natl Acad Sci U S A 1996;93:7849–54.
[22] Lee JE, Beck TW, Brennscheidt U, DeGennaro LJ, Rapp UR. The complete sequence and promoter activity of the human A-raf-1 gene (ARAF1). Genomics 1994;20:43–55.
[23] Olofsson B, Pajusola K, Kaipainen A, et al. Vascular endothelial growth factor B, a novel growth factor for endothelial cells. Proc Natl Acad Sci U S A 1996;93:2576–81.
[24] Maekawa M, Ishizaki T, Boku S, et al. Signaling from Rho to the actin cytoskeleton through protein kinases ROCK and LIM-kinase. Science 1999;285:895–8.
[25] Baumer AT, Flesch M, Wang X, Shen Q, Feuerstein GZ, Bohm M. Antioxidative enzymes in human hearts with idiopathic dilated cardiomyopathy. J Mol Cell Cardiol 2000;32:121–30.
[26] Ohkusa T, Ueyama T, Yamada J, et al. Alterations in cardiac sarcoplasmic reticulum Ca^{2+} regulatory proteins in the atrial tissue of patients with chronic atrial fibrillation. J Am Coll Cardiol 1999;34:255–63.
[27] van der Velden HM, Ausma J, Rook MB, et al. Gap junctional remodeling in relation to stabilization of atrial fibrillation in the goat. Cardiovasc Res 2000;46:476–86.
[28] Brundel BJ, van Gelder IC, Henning RH, et al. Gene expression of proteins influencing the calcium homeostasis in patients with persistent and paroxysmal atrial fibrillation. Cardiovasc Res 1999;42:443–54.
[29] Brundel BJ, VanGelder IC, Henning RH, et al. Alterations in potassium channel gene expression in atria of patients with persistent and paroxysmal atrial fibrillation: differential regulation of protein and mRNA levels for K+channels. J Am Coll Cardiol 2001;37:926–32.

Oncogene (2006) 25, 139–146

www.nature.com/onc

SHORT COMMUNICATION

Epigenetic silencing of *AXIN2* in colorectal carcinoma with microsatellite instability

K Koinuma[1,2], Y Yamashita[1], W Liu[3], H Hatanaka[1], K Kurashina[1,2], T Wada[1], S Takada[1], R Kaneda[1], YL Choi[1], S-I Fujiwara[1], Y Miyakura[2], H Nagai[2] and H Mano[1,4]

[1]Division of Functional Genomics, Jichi Medical School, Tochigi, Japan; [2]Department of Surgery, Jichi Medical School, Tochigi, Japan; [3]Division of Experimental Pathology, Mayo Clinic and Mayo Medical School, Rochester, MN, USA and [4]CREST, Japan Science and Technology Agency, Saitama, Japan

Mutation or epigenetic silencing of mismatch repair genes, such as *MLH1* and *MSH2*, results in microsatellite instability (MSI) in the genome of a subset of colorectal carcinomas (CRCs). However, little is yet known of genes that directly contribute to tumor formation in such cancers. To characterize MSI-dependent changes in gene expression, we have now compared transcriptomes between fresh CRC specimens positive or negative for MSI ($n = 10$ for each) with the use of high-density oligonucleotide microarrays harboring >44 000 probe sets. Correspondence analysis of the expression patterns of isolated MSI-associated genes revealed that the transcriptome of MSI$^+$ CRCs is clearly distinct from that of MSI$^-$ CRCs. Such MSI-associated genes included that for AXIN2, an important component of the WNT signaling pathway. *AXIN2* was silenced, apparently as a result of extensive methylation of its promoter region, specifically in MSI$^+$ CRC specimens. Forced expression of *AXIN2*, either by treatment with 5′-azacytidine or by transfection with *AXIN2* cDNA, resulted in rapid cell death in an MSI$^+$ CRC cell line. These data indicate that epigenetic silencing of *AXIN2* is specifically associated with carcinogenesis in MSI$^+$ CRCs.

Oncogene (2006) **25**, 139–146. doi:10.1038/sj.onc.1209009; published online 10 October 2005

Keywords: epigenetics; colorectal carcinoma; microsatellite instability; AXIN2; MLH1

Colorectal carcinoma (CRC) is one of the leading causes of cancer death in humans. Evidence indicates the existence of two major types of genomic instability in CRCs: chromosomal instability and microsatellite instability (MSI) (Lengauer *et al.*, 1998). Whereas chromosomal instability is associated with an abnormal DNA content (such as aneuploidy), inactivation of the tumor suppressor gene *TP53*, and activation of oncogenes (Kinzler and Vogelstein, 1996), MSI is associated with defects in DNA mismatch repair (MMR) that result in frameshift mutations in microsatellite repeats and thereby affect the structure of genes containing such repeats (Ionov *et al.*, 1993).

Although germline mutations of MMR genes have been detected in the genome of individuals with hereditary nonpolyposis colorectal cancer (Fishel *et al.*, 1993; Bronner *et al.*, 1994; Papadopoulos *et al.*, 1994), many sporadic CRCs positive for MSI are associated with epigenetic silencing of nonmutated MMR genes (Toyota *et al.*, 1999; Miyakura *et al.*, 2001). MSI$^+$ CRCs are characterized by specific clinicopathologic features and gene mutations. They occur with a higher frequency in women than in men, develop in the right side of the colon, and manifest a mucinous or poorly differentiated histopathology. Many of the CpG dinucleotides within the promoter region of the MMR gene *MLH1* are methylated (Cunningham *et al.*, 1998; Veigl *et al.*, 1998) and the *BRAF* gene frequently contains activating mutations (Koinuma *et al.*, 2004) in MSI$^+$ CRCs. Multiple genomic fragments have been found to be methylated in such CRCs (Toyota *et al.*, 1999), and an entity of CRC with a CpG island methylator phenotype has been proposed (Issa, 2004). The repertoire of genes that become methylated specifically in CRCs positive for *MLH1* methylation has remained uncharacterized, however.

To characterize directly the transcriptome specifically associated with MSI$^+$ CRC, we have now compared transcriptomes between fresh CRC specimens with or without MSI. Unexpectedly, we found that the expression of *AXIN2*, which encodes a component of the WNT signaling pathway, was markedly suppressed among the former tumors. CpG sequences within the *AXIN2* promoter were revealed to be extensively methylated in such CRCs. Forced expression of *AXIN2* inhibited cell proliferation in an MSI$^+$ CRC cell line, indicating that loss of *AXIN2* transcription is directly associated with carcinogenesis in MSI$^+$ CRCs.

To identify genes whose expression is specifically altered in MSI$^+$ CRCs, we first compared the transcriptomes of CRCs with or without MSI. A total of 248 consecutive cases of CRC were examined for MSI status

Correspondence: Professor H Mano, Division of Functional Genomics, Jichi Medical School, 3311-1 Yakushiji, Kawachigun, Tochigi 329-0498, Japan.
E-mail: hmano@jichi.ac.jp
Received 28 April 2005; revised 7 July 2005; accepted 13 July 2005; published online 10 October 2005

as well as for methylation of the promoter region of *MLH1* (Koinuma *et al.*, 2004). Most ($n=213$) of the cancer specimens were MSI$^-$, with the remainder ($n=35$) being positive for MSI. To compare the transcriptomes of these two subtypes of CRC, we randomly selected 10 specimens from each group and subjected them to gene expression profiling with microarrays (Affymetrix GeneChip HGU133) that harbor >44 000 probe sets. The clinical characteristics of the patients whose CRC specimens were subjected to microarray analysis are summarized in Table 1.

To exclude transcriptionally silent genes from our analyses, we first chose probe sets that received the 'Present' call from Microarray Suite 5.0 (Affymetrix) in at least 10% ($n=2$) of the samples. Two-way hierarchical clustering (Alon *et al.*, 1999) of the 20 patients based on the expression profiles of the isolated 21 888 probe sets failed to separate those with MSI$^+$ CRC from those with MSI$^-$ CRC (data not shown). We therefore attempted to identify 'MSI-associated probe sets' whose expression intensities differed significantly (Student's *t*-test, $P<0.001$) between the two classes and whose effect size (absolute difference in mean expression level) was $\geqslant 50$ U. Two-way clustering analysis with the 24 probe sets that fulfilled both these criteria clearly separated the individuals of the two clinical classes (Figure 1a). The distinct transcriptomes of the two classes were also confirmed by correspondence analysis (Fellenberg *et al.*, 2001), which reduced the complexity of the gene expression patterns from 24 to three dimensions. Projection of the study subjects into a virtual three-dimensional space based on their calculated coordinates revealed that the MSI$^+$ specimens were positioned apart from the MSI$^-$ ones (Figure 1b). These data indicate that the two classes of CRC possess distinct gene expression profiles, or 'molecular signatures', and they also suggest the feasibility of gene expression-based differential diagnosis of the two CRC subtypes.

Table 1 Clinical characteristics of the study subjects enrolled in microarray analysis

Patient ID	*Age (years)*	*Sex*	*MSI status*	MLH1 *methylation*	BRAF *gene*	KRAS2 *gene*	*Tumor site*	*Dukes stage*	*Pathology*	AXIN2 *methylation*
225	83	Female	Positive	Yes	Mutant	Wild	Proximal	C	Well	Yes
263	86	Female	Positive	Yes	Mutant	Wild	Proximal	C	Mod	Yes
280	83	Female	Positive	Yes	Mutant	Wild	Proximal	C	Well	Yes
305	74	Male	Positive	Yes	Mutant	Wild	Proximal	B	Sig	No
318	76	Female	Positive	Yes	Mutant	Wild	Proximal	B	Well	Yes
336	68	Male	Positive	Yes	Mutant	Wild	Proximal	B	Muc	No
413	69	Female	Positive	Yes	Mutant	Wild	Proximal	A	Well	No
416	76	Female	Positive	Yes	Mutant	Wild	Proximal	B	Muc	No
433	54	Female	Positive	Yes	Wild	Wild	Proximal	D	Well	Yes
479	74	Female	Positive	Yes	Mutant	Wild	Proximal	B	Mod	No
238	74	Male	Negative	No	Wild	Mutant	Distal	A	Well	No
249	62	Male	Negative	No	Wild	Wild	Proximal	B	Well	No
278	73	Male	Negative	No	Wild	Wild	Proximal	C	Well	No
295	71	Female	Negative	No	Wild	Mutant	Proximal	C	Well	No
298	70	Male	Negative	No	Wild	Mutant	Proximal	D	Well	No
307	80	Female	Negative	No	Wild	Wild	Proximal	C	Mod	No
308	62	Male	Negative	No	Wild	Wild	Distal	B	Mod	No
319	53	Female	Negative	No	Wild	Wild	Distal	A	Well	No
419	45	Female	Negative	No	Wild	Mutant	Proximal	D	Muc	No
426	42	Female	Negative	No	Wild	Wild	Proximal	C	Well	No

Well = well-differentiated adenocarcinoma; Mod = moderately differentiated adenocarcinoma; Sig = signet ring cell adenocarcinoma; Muc = mucinous adenocarcinoma. Methylation of *AXIN2* promoter region was determined by COBRA method.

Figure 1 Comparison of transcriptomes between CRCs positive or negative for MSI. (**a**) Subject tree generated by two-way clustering analysis with 24 probe sets that contrasted the two clinical conditions ($P<0.001$; effect size, $\geqslant 50$ U). Tumor samples were obtained from individuals with sporadic CRC who underwent surgical treatment at Jichi Medical School Hospital. Written informed consent was obtained from all patients, and the present study was approved by the ethics committee of Jichi Medical School. Microsatellite stability was determined by analysis of nine microsatellite repeat loci (three dinucleotide repeats and six mononucleotide repeats) as described previously (Miyakura *et al.*, 2001), and MSI status was stratified according to the criteria of the National Cancer Institute workshop (Boland *et al.*, 1998). Total RNA was extracted from ~100 mg of tissue, and was used in the hybridization experiments with GeneChip HGU133 A&B microarrays (Affymetrix), which harbor >44 000 probe sets corresponding to ~33 000 human genes, as described previously (Ohki-Kaneda *et al.*, 2004). The mean expression intensity of the internal positive control probe sets (http://www.affymetrix.com/support/technical/mask_files.affx) on the microarrays was set to 500 units (U) in each hybridization, and the fluorescence intensity of each probe set was normalized accordingly. All normalized array data are available at the Gene Expression Omnibus website (http://www.ncbi.nlm.nih.gov/geo) under the Accession Number GSE2138. Each column corresponds to a separate sample (MSI$^-$, green; MSI$^+$, red), and each row to a probe set whose expression is color-coded according to the indicated scale. Gene symbols are shown on the right; 225541_at, 226545_at, and 242414_at are expressed sequence tag IDs designated by Affymetrix (http://www.affymetrix.com). Annotations and expression intensities for the probe sets are presented in Supplementary Table 1. Note that *MLH1* expression was specifically suppressed in the MSI$^+$ samples. (**b**) Samples were projected into a virtual space with coordinates calculated by correspondence analysis of the 24 probe sets shown in (**a**). Correspondence analysis was performed with ViSta software (http://www.visualstats.org) for all genes showing a significant difference.

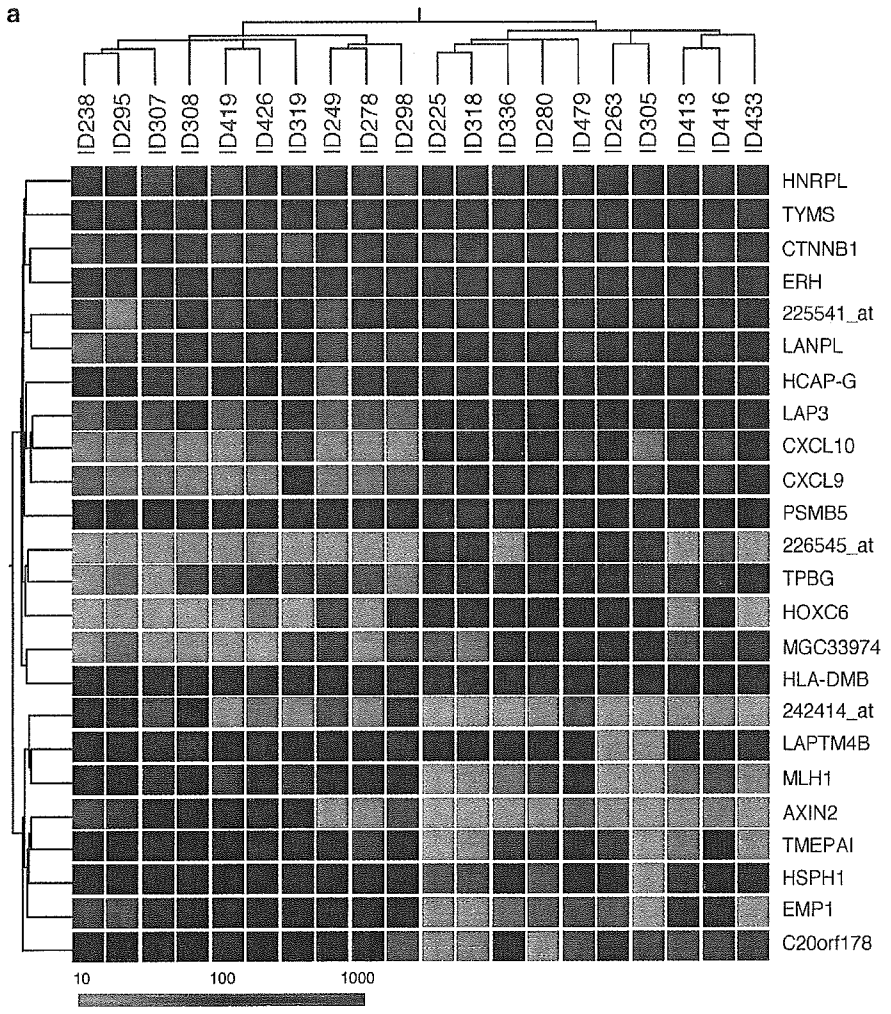
a
ID238
ID295
ID307
ID308
ID419
ID426
ID319
ID249
ID278
ID298
ID225
ID318
ID336
ID280
ID479
ID263
ID305
ID413
ID416
ID433
HNRPL
TYMS
CTNNB1
ERH
225541_at
LANPL
HCAP-G
LAP3
CXCL10
CXCL9
PSMB5
226545_at
TPBG
HOXC6
MGC33974
HLA-DMB
242414_at
LAPTM4B
MLH1
AXIN2
TMEPAI
HSPH1
EMP1
C20orf178
10
100
1000
b
0.6
0.4
0.2
0.0
-0.2
-0.4
-0.6
-0.8
1st dimension
MSI-positive
MSI-negative
0.4
0.2
0.0
-0.2
-0.4
2nd dimension
-0.3
-0.2
-0.1
0.0
0.1
0.2
0.3
0.4
3rd dimension

The isolated MSI-associated genes include *AXIN2* and *CTNNB1* (β-catenin), both of which encode key participants in the WNT signaling pathway (Tolwinski and Wieschaus, 2004). Dysregulation of ubiquitin-dependent degradation of β-catenin contributes to carcinogenesis in a variety of CRCs and hepatocellular carcinomas (Narayan and Roy, 2003). AXIN2, similar to AXIN1, functions as a scaffold protein to facilitate this ubiquitination process by recruiting adenomatous polyposis coli (APC), glycogen synthase kinase-3β, and β-catenin (Behrens *et al*., 1998). Defects in the degradation of β-catenin have been shown to result from mutations in *AXIN1*, *AXIN2*, *APC*, or *CTNNB1* (Rubinfeld *et al*., 1997; Liu *et al*., 2000; Satoh *et al*., 2000; Smith *et al*., 2002). Our data therefore suggest that transcriptional suppression of *AXIN2* might represent a novel mechanism by which the function of the APC-AXIN–β-catenin complex is impaired in CRC.

To confirm the MSI-associated change in *AXIN2* expression, we measured the abundance of the corresponding mRNA in the original 20 study specimens by quantitative reverse transcription–polymerase chain reaction (RT–PCR) analysis (Figure 2a). Comparison of the amount of *AXIN2* mRNA determined by RT–PCR with that determined by microarray analysis yielded a Pearson's correlation coefficient (r) of 0.89, indicating that the two data sets were highly correlated ($P<0.001$). (Also see Supplementary Figure 1 for verification of microarray data by RT–PCR.)

With the use of RT–PCR, we then measured the amount of *AXIN2* mRNA in a larger number of samples (seven additional specimens of MSI$^+$ CRC, for a total of 17; 10 additional specimens of MSI$^-$ CRC, for a total of 20; three MSI$^+$ CRC cell lines; two MSI$^-$ CRC cell lines). The abundance of *AXIN2* transcripts in most of the MSI$^+$ CRC specimens and cell lines was reduced compared with that in the MSI$^-$ ones (Figure 2b); an *AXIN2*/*ACTB* transcript ratio of $<5\times10^{-4}$ was apparent in 13 of the 17 MSI$^+$ CRC specimens, but in only five of the 20 MSI$^-$ ones (Fisher's exact probability test, $P=0.003$). Importantly, a similar MSI-dependent suppression of *AXIN1* expression was not observed among these specimens ($P=0.31$) (data not shown).

Human *AXIN2* possesses a relatively large CpG island within its promoter region (nucleotide positions, chr17: 60986365–60987824). We therefore examined the methylation status of the CpG sites within this region by nucleotide sequencing after sodium bisulfite treatment. Extensive methylation of the CpG island in the *AXIN2* promoter was apparent in CRC specimens positive for MSI and for the loss of *AXIN2* expression (Figure 2c). The promoter region in the MSI$^+$ CRC cell line HCT116 (Wheeler *et al*., 1999) was also heavily methylated. The *MLH1* promoter in HCT116 cells is not methylated, but the coding sequence of the gene contains a mutation that results in MSI (Wheeler *et al*., 1999).

On the basis of these findings, we examined the methylation status of the *AXIN2* promoter in 37 clinical specimens and five cell lines by combined bisulfite restriction analysis (COBRA) (Xiong and Laird, 1997). CpG methylation was detected in five of the 17 MSI$^+$ specimens, but in none of the 20 MSI$^-$ specimens (Table 1; see Supplementary Table 2). Methylation of the *AXIN2* promoter was not detected in normal colon tissue obtained from the individuals with MSI$^+$ CRC (data not shown), suggesting that *AXIN2* methylation was a somatic event in these patients.

We then tested whether the amount of the encoded protein correlated with that of *AXIN2* mRNA in CRC specimens (Figure 2d). Immunohistochemical staining showed that AXIN2 was abundant in a specimen with a high mRNA content (ID308), but was present in much smaller amounts in two specimens with a low mRNA content (ID263, ID295). Although a large amount of *AXIN2* mRNA was not always associated with a large amount of protein, a small amount of mRNA was consistently associated with a small amount of protein (data not shown).

To examine directly whether epigenetic silencing of *AXIN2* is relevant to the change in the growth properties of CRC cells, we restored *AXIN2* expression, either by 5′-azacytidine treatment or by introduction of *AXIN2* cDNA, in an MSI$^+$ CRC cell line. 5′-Azacytidine inhibits *de novo* methylation of genomic DNA and thereby induces demethylation of the genome of proliferating cells (Christman, 2002). HCT116 cells were incubated for 3 days with various concentrations of 5′-azacytidine and were then subjected to COBRA for determination of the methylation status of the *AXIN2* promoter. Treatment with 5′-azacytidine reduced the level of methylation of the *AXIN2* promoter in a concentration-dependent manner (Figure 3a). This effect of 5′-azacytidine was accompanied by an increase in the amount of *AXIN2* mRNA in the cells (Figure 3b) as well as by the induction of cell death (Figure 3c).

Given that 5′-azacytidine likely affects the transcription of other genes in addition to that of *AXIN2*, the growth inhibitory effect observed in HCT116 cells might not have been attributable solely to the induction of *AXIN2* expression. To examine the direct effect of *AXIN2*, we introduced its cDNA into HCT116 cells by transfection. However, an introduction of *AXIN2* cDNA (even with the use of an inducible system) resulted in rapid cell death, and we could not establish stable transformants of cell lines with such expression constructs (data not shown). Therefore, we generated an amphotropic recombinant retrovirus that confers simultaneous expression of both an MYC epitope-tagged form of AXIN2 and mouse CD8. Human kidney 293 cells infected with this virus, but not those infected with a mock virus, expressed AXIN2 (Figure 3d). HCT116 cells were then infected with the virus and were subjected to affinity chromatography 48 h thereafter to isolate cells that express CD8. Given that CD8-expressing cells would be expected also to express AXIN2, this column purification step should result in rapid enrichment of AXIN2-expressing cells. The isolated cells indeed contained a substantial amount of *AXIN2* mRNA as revealed by RT–PCR (Figure 3e). The purified CD8$^+$ HCT116 cells were then cultured for 3 days to characterize their growth properties. Forced expression of AXIN2 resulted in marked inhibition of cell growth

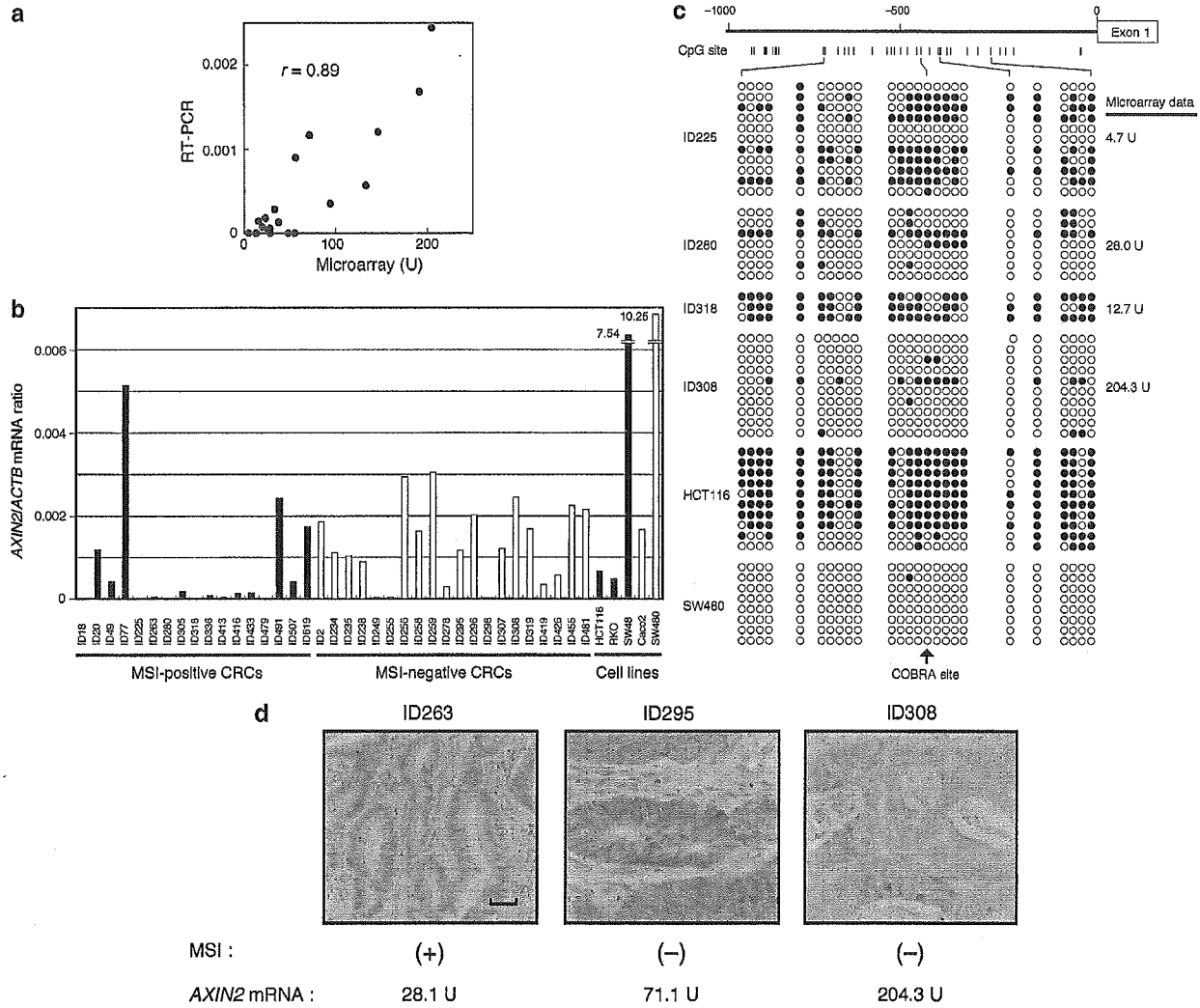

Figure 2 Suppression of *AXIN2* expression in CRCs positive for MSI. (**a**) Comparison of the abundance of *AXIN2* mRNA in study specimens as determined by microarray and RT–PCR analyses. For the latter, the amount of *AXIN2* mRNA was expressed relative to that of *ACTB* mRNA. Pearson's correlation coefficient (*r*) for the comparison is indicated. Portions of double-stranded cDNA were subjected to PCR with a QuantiTect SYBR Green PCR Kit (Qiagen). The amplification protocol comprised incubations at 94°C for 15 s, 63°C for 30 s, and 72°C for 60 s. Incorporation of the SYBR Green dye into PCR products was monitored in real time with an ABI PRISM 7700 sequence detection system (PE Applied Biosystems), thereby allowing determination of the threshold cycle (C_T) at which exponential amplification of products begins. The amount of target cDNAs relative to that of the β-actin (*ACTB*) cDNA was calculated from the C_T values with the use of Sequence Detector ver. 1.6.3 software (PE Applied Biosystems). The primers used for PCR amplification were 5′-CTGGCTCCAGAAGATCACAAAG-3′ and 5′-ATCTCCTCAAACACCGCTCCA-3′ for *AXIN2* and 5′-CCATCATGAAGTGTGACGTGG-3′ and 5′-GTCCGCCTAGAAGCATTTGCG-3′ for *ACTB*. (**b**) Comparison of the amount of *AXIN2* mRNA relative to that of *ACTB* mRNA (as determined by RT–PCR) between MSI$^+$ (closed bars) and MSI$^-$ (open bars) CRC specimens and cell lines. (**c**) Genomic DNA of the indicated clinical specimens and CRC cell lines was treated with sodium bisulfite (Koinuma *et al*., 2004), after which the *AXIN2* promoter region was amplified by PCR with the primers 5′-TTGTATATAGTTTA GYGGTTGGG-3′ and 5′-AAATCTAAACTCCCTACACACTT-3′. Closed and open circles indicate methylated and unmethylated CpG sites, respectively. The positions of the CpG sites are indicated at the top, the *Hha*I digestion site for COBRA is indicated by the arrow, and the microarray data for *AXIN2* expression are shown on the right. (**d**) Immunohistochemical analysis of the indicated clinical specimens with antibodies to AXIN2. The MSI status and the expression level of *AXIN2* determined by microarray analysis are indicated. Immunohistochemical analysis of AXIN2 expression was performed as described previously (Leung *et al*., 2002). Sections (5 μm) of formalin-fixed, paraffin-embedded tissue were mounted on Probe-On slides (Fisher Scientific), which were then incubated first for 1 h at room temperature with 1.5% normal horse serum and then overnight at 4°C with goat polyclonal antibodies to AXIN2 (Santa Cruz Biotechnology). Immune complexes were detected by the avidin–biotin–peroxidase method with 3,3′-diaminobenzidine as the chromogenic substrate (Vectastain ABC kit, Vector Laboratories). The sections were counterstained with hematoxylin. Scale bar, 50 μm.

(Figure 3f), indicating that silencing of *AXIN2* is indeed relevant to tumorigenesis. We also examined if the expression of *AXIN2* directly suppresses the WNT signaling pathway. For this purpose, we utilized a luciferase-based reporter plasmid (TOPflash) for the T-cell factor (TCF) activity, which is a direct target of

β-catenin (Korinek *et al.*, 1997). As shown in Figure 3g, a forced expression of *AXIN2* induced a marked suppression in the luciferase activity in HCT116 cells. On the other hand, *AXIN2* did not affect luciferase activity driven by a mutated, nonfunctional TCF-binding sites (FOPflash). These data clearly indicate that AXIN2 is involved in the WNT–APC–β-catenin pathway in CRCs.

We have demonstrated preferential transcriptional silencing of *AXIN2* in MSI$^+$ CRCs. Recently, mutations within exon 7 of the *AXIN2* gene have been reported in MSI$^+$ CRC specimens (Liu *et al.*, 2000; Wu *et al.*, 2001). We have thus analysed the nucleotide sequence of the *AXIN2* gene among our MSI$^+$ samples ($n=9$). Sequencing of the *AXIN2* exon 7 has revealed that only one patient (ID no. 263) carried a mutated *AXIN2* gene in one allele (data not shown). A deletion of a cytosine residue at the nucleotide position 2096 of the *AXIN2* cDNA (GenBank Accession Number, AF078165) led to a frame shift in the open-reading frame in this patient, introducing a premature termination codon in AXIN2 protein at the amino-acid position of 688. However, majority of the patients had intact *AXIN2* genes, indicating that silencing, but not mutation, of *AXIN2* is the main pathway to impede the *AXIN2* function.

The COBRA experiments revealed that the promoter region of *AXIN2* was extensively methylated in MSI$^+$ CRCs but not in MSI$^-$ CRCs. Although the difference in the frequency of *AXIN2* methylation between these two classes of tumor was significant (Fisher's exact probability test, $P=0.003$), the frequency for the MSI$^+$ specimens was still only 29% and therefore was not able to account for all the observed instances of suppression of *AXIN2* expression. We judged COBRA data as positive for methylation if $\geqslant 10\%$ of the PCR products were digested by *Hha*I. However, a small proportion ($<10\%$) of the PCR products was digested in the analysis of $\sim 50\%$ of MSI$^+$ CRC specimens (data not shown), indicating that alterations in the methylation status of the *AXIN2* promoter were more widespread. It is therefore possible that CpG sites other than that targeted by COBRA are more frequently methylated in MSI$^+$ CRCs and are more important for transcriptional regulation.

Similar promoter methylation has been recently described for other genes important for the WNT signaling pathway. The genes for secreted frizzled-related proteins are thus epigenetically silenced in MSI$^+$ CRCs, resulting in constitutive activation of the WNT pathway (Suzuki *et al.*, 2004). CpG sites within the *APC* promoter were also found to be frequently methylated in CRCs and other cancers (Esteller *et al.*, 2000; Zysman *et al.*, 2002). These data thus suggest that not only genetic mutations but also epigenetic silencing might play an important role in tumorigenesis mediated by activation of the WNT pathway.

Methylation of the *APC* promoter in endometrial cancer has been shown to occur preferentially in MSI$^+$ tumors (Zysman *et al.*, 2002). Despite the lack of an MSI-associated difference in the expression of *APC* in our CRC specimens (data not shown), the results of this previous study together with our present findings suggest the possibility that genes related to the WNT signaling pathway are targeted for methylation specifically in cancers with MSI. Our data further indicate that such methylation in MSI$^+$ cancers may be directly relevant to the mechanism of malignant transformation through epigenetic silencing of tumor suppressor genes. MSI$^+$ CRCs have been thought to arise through genetic events distinct from those that underlie MSI$^-$ cancers (Rajagopalan and Lengauer, 2004), which are frequently associated with aneuploidy and mutations in WNT pathway genes such as *APC* and *CTNNB1*. However, our data indicate that the molecular mechanisms for malignant transformation overlap between MSI$^+$ and MSI$^-$ CRCs.

Figure 3 Induction of cell death by restoration of *AXIN2* expression in a CRC cell line with a methylated *AXIN2* promoter. (**a**) HCT116 cells were incubated for 72 h with 0, 0.2, or 1 μM 5′-azacytidine and were then subjected to COBRA for determination of the methylation status of the *AXIN2* promoter (Xiong and Laird, 1997). Genomic DNA was denatured, incubated for 16 h at 55°C in 3.1 M sodium bisulfite, and then subjected to PCR with the primers in Figure 2c. The PCR products were then digested with the restriction endonuclease *Hha*I (Takara Bio), and the resulting DNA fragments were fractionated by polyacrylamide gel electrophoresis. The gel was stained with SYBR Green I (Takara Bio) and scanned with an LAS3000 imaging system (Fuji Film). Genomic fragments were determined to be positive for CpG methylation if $\geqslant 10\%$ of the PCR products were cleaved by the restriction endonuclease. Lane M, DNA size markers (50-bp ladder). (**b**) The cells from (**a**) were also subjected to RT–PCR analysis for determination of the amount of *AXIN2* mRNA relative to that of *ACTB* mRNA. (**c**) Cells treated as in (**a**) with 0, 0.2, 1, or 5 μM 5′-azacytidine were examined by light microscopy. Cell death was estimated by counting the remaining viable cells in each culture dish by the dye-exclusion method. Scale bar, 50 μm. (**d**) Human kidney 293 cells infected with either a mock virus or a recombinant virus encoding both MYC epitope-tagged AXIN2 and mouse CD8. A human cDNA for AXIN2 tagged at its NH_2-terminus with the MYC epitope sequence was ligated into the pMX-iresCD8 retroviral plasmid (Yamashita *et al.*, 2001) to yield pMX-AXIN2-MYC-iresCD8. The latter plasmid was introduced into BOSC23 cells together with pE-ampho and pGP packaging plasmids (Takara Bio) by transfection with the use of Lipofectamine (Invitrogen). The culture supernatant containing recombinant viruses was added to 293 cells with 4 μg/ml of polybrene (Sigma). Cells were then subjected to immunoprecipitation with the antibodies to MYC (9E10, Roche Diagnostics), and to immunoblot analysis with the same antibodies. (**e**) HCT116 cells infected with the viruses in (**d**) were subjected to affinity chromatography to isolate CD8$^+$ cells, which were then subjected to RT–PCR analysis for quantitation of *AXIN2* mRNA relative to the amount of *ACTB* mRNA. (**f**) The CD8$^+$ fractions in (**e**) were seeded at a density of 5×10^4 cells/dish and cultured for 72 h, after which the ratio of the final cell number to the initial value was determined. Data are means + s.d. of triplicate from a representative experiment. The *P*-value for the indicated comparison was determined by Student's *t* test. (**g**) HCT116 cells were seeded at a density of 2.5×10^6 cells/6 cm dish. After 24 h of incubation, the cells were transfected, with the use of Lipofectamine, with 2 μg of pMX-AXIN2-MYC-iresCD8 (AXIN2) or pMX-iresCD8 (Mock). For the reporter plasmids, 0.5 μg of pGL4 (Promega, Madison, WI, USA) plus either 0.5 μg of pTOPflash or 0.5 μg of pFOPflash (both from Upstate Biotechnology, Lake Placid, NY, USA) were added to the lipofection mix. The activity of *Photinus pyralis* luciferase was measured after 24 h of incubation with the use of the Dual-luciferase reporter assay system (Promega), and normalized on the basis of the activity of *Renilla reniformis* luciferase produced by pGL4. Data are shown as the mean value + s.d. of triplicate samples.

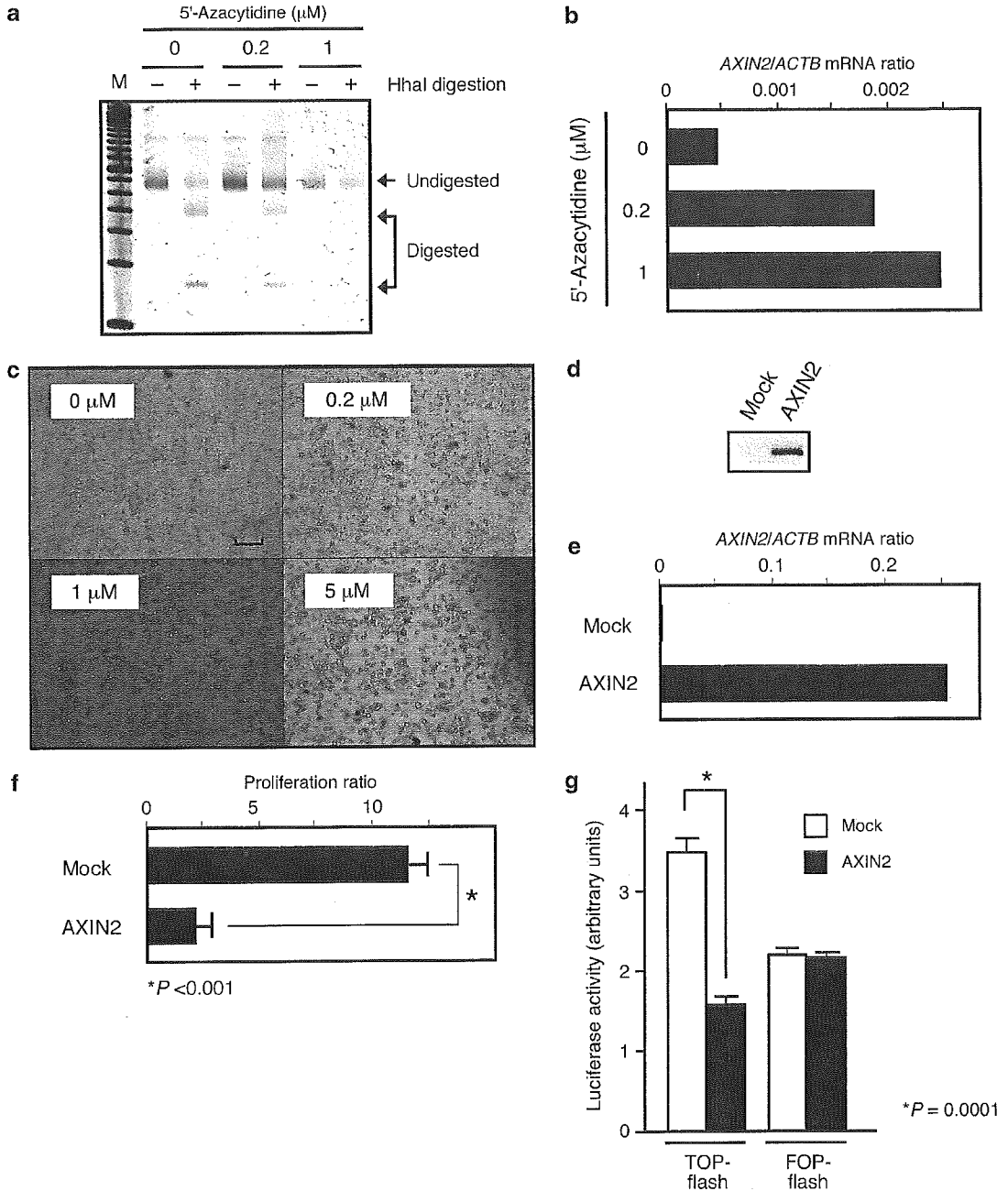

Acknowledgements

We thank M Toyota and SN Thibodeau for critical reading of the manuscript and helpful suggestions. This study was supported in part by a grant for Third-Term Comprehensive Control Research for Cancer from the Ministry of Health, Labor, and Welfare of Japan, and by a grant for 'High-Tech Research Center' Project for Private Universities: Matching Fund Subsidy (2002–2006) from the Ministry of Education, Culture, Sports, Science, and Technology of Japan.

References

Alon U, Barkai N, Notterman DA, Gish K, Ybarra S, Mack D *et al.* (1999). *Proc Natl Acad Sci USA* **96**: 6745–6750.

Behrens J, Jerchow BA, Wurtele M, Grimm J, Asbrand C, Wirtz R *et al.* (1998). *Science* **280**: 596–599.

Boland CR, Thibodeau SN, Hamilton SR, Sidransky D, Eshleman JR, Burt RW *et al.* (1998). *Cancer Res* **58**: 5248–5257.

Bronner CE, Baker SM, Morrison PT, Warren G, Smith LG, Lescoe MK *et al.* (1994). *Nature* **368**: 258–261.

Christman JK. (2002). *Oncogene* **21**: 5483–5495.
Cunningham JM, Christensen ER, Tester DJ, Kim CY, Roche PC, Burgart LJ *et al.* (1998). *Cancer Res* **58**: 3455–3460.
Esteller M, Sparks A, Toyota M, Sanchez-Cespedes M, Capella G, Peinado MA *et al.* (2000). *Cancer Res* **60**: 4366–4371.
Fellenberg K, Hauser NC, Brors B, Neutzner A, Hoheisel JD, Vingron M. (2001). *Proc Natl Acad Sci USA* **98**: 10781–10786.
Fishel R, Lescoe MK, Rao MR, Copeland NG, Jenkins NA, Garber J *et al.* (1993). *Cell* **75**: 1027–1038.
Ionov Y, Peinado MA, Malkhosyan S, Shibata D, Perucho M. (1993). *Nature* **363**: 558–561.
Issa JP. (2004). *Nat Rev Cancer* **4**: 988–993.
Kinzler KW, Vogelstein B. (1996). *Cell* **87**: 159–170.
Koinuma K, Shitoh K, Miyakura Y, Furukawa T, Yamashita Y, Ota J *et al.* (2004). *Int J Cancer* **108**: 237–242.
Korinek V, Barker N, Morin PJ, van Wichen D, de Weger R, Kinzler KW *et al.* (1997). *Science* **275**: 1784–1787.
Lengauer C, Kinzler KW, Vogelstein B. (1998). *Nature* **396**: 643–649.
Leung JY, Kolligs FT, Wu R, Zhai Y, Kuick R, Hanash S *et al.* (2002). *J Biol Chem* **277**: 21657–21665.
Liu W, Dong X, Mai M, Seelan RS, Taniguchi K, Krishnadath KK *et al.* (2000). *Nat Genet* **26**: 146–147.
Miyakura Y, Sugano K, Konishi F, Ichikawa A, Maekawa M, Shitoh K *et al.* (2001). *Gastroenterology* **121**: 1300–1309.
Narayan S, Roy D. (2003). *Mol Cancer* **2**: 41.
Ohki-Kaneda R, Ohashi J, Yamamoto K, Ueno S, Ota J, Choi YL *et al.* (2004). *Biochem Biophys Res Commun* **320**: 1328–1336.
Papadopoulos N, Nicolaides NC, Wei YF, Ruben SM, Carter KC, Rosen CA *et al.* (1994). *Science* **263**: 1625–1629.
Rajagopalan H, Lengauer C. (2004). *Nature* **432**: 338–341.
Rubinfeld B, Robbins P, El-Gamil M, Albert I, Porfiri E, Polakis P. (1997). *Science* **275**: 1790–1792.
Satoh S, Daigo Y, Furukawa Y, Kato T, Miwa N, Nishiwaki T *et al.* (2000). *Nat Genet* **24**: 245–250.
Smith G, Carey FA, Beattie J, Wilkie MJ, Lightfoot TJ, Coxhead J *et al.* (2002). *Proc Natl Acad Sci USA* **99**: 9433–9438.
Suzuki H, Watkins DN, Jair KW, Schuebel KE, Markowitz SD, Dong Chen W *et al.* (2004). *Nat Genet* **36**: 417–422.
Tolwinski NS, Wieschaus E. (2004). *Trends Genet* **20**: 177–181.
Toyota M, Ahuja N, Ohe-Toyota M, Herman JG, Baylin SB, Issa JP. (1999). *Proc Natl Acad Sci USA* **96**: 8681–8686.
Veigl ML, Kasturi L, Olechnowicz J, Ma AH, Lutterbaugh JD, Periyasamy S *et al.* (1998). *Proc Natl Acad Sci U S A* **95**: 8698–8702.
Wheeler JM, Beck NE, Kim HC, Tomlinson IP, Mortensen NJ, Bodmer WF. (1999). *Proc Natl Acad Sci USA* **96**: 10296–10301.
Wu R, Zhai Y, Fearon ER, Cho KR. (2001). *Cancer Res* **61**: 8247–8255.
Xiong Z, Laird PW. (1997). *Nucleic Acids Res* **25**: 2532–2534.
Yamashita Y, Kajigaya S, Yoshida K, Ueno S, Ota J, Ohmine K *et al.* (2001). *J Biol Chem* **276**: 39012–39020.
Zysman M, Saka A, Millar A, Knight J, Chapman W, Bapat B. (2002). *Cancer Res* **62**: 3663–3666.

Supplementary Information accompanies the paper on Oncogene website (http://www.nature.com/onc).

Available online at www.sciencedirect.com
SCIENCE DIRECT®
ELSEVIER
Biochemical and Biophysical Research Communications 338 (2005) 1256–1262
BBRC
www.elsevier.com/locate/ybbrc

Transforming activity of the lymphotoxin-β receptor revealed by expression screening

Shin-ichiro Fujiwara [a,b,c], Yoshihiro Yamashita [a], Young Lim Choi [a], Tomoaki Wada [a], Ruri Kaneda [a,d], Shuji Takada [a], Yukio Maruyama [c], Keiya Ozawa [b], Hiroyuki Mano [a,d,*]

[a] *Division of Functional Genomics, Jichi Medical School, Tochigi 329-0498, Japan*
[b] *Division of Hematology, Jichi Medical School, Tochigi 329-0498, Japan*
[c] *First Department of Internal Medicine, Fukushima Medical University, Fukushima 960-1295, Japan*
[d] *CREST, Japan Science and Technology Agency, Saitama 332-0012, Japan*

Received 13 October 2005
Available online 24 October 2005

Abstract

Pancreatic ductal carcinoma (PDC) remains one of the most intractable human malignancies. To obtain insight into the molecular pathogenesis of PDC, we constructed a retroviral cDNA expression library with total RNA isolated from the PDC cell line MiaPaCa-2. Screening of this library with the use of a focus formation assay with NIH 3T3 mouse fibroblasts resulted in the identification of 13 independent genes with transforming activity. One of the cDNAs thus identified encodes an NH_2-terminally truncated form of the lymphotoxin-β receptor (LTBR). The transforming activity of this short-type LTBR in 3T3 cells was confirmed by both an in vitro assay of cell growth in soft agar and an in vivo assay of tumorigenicity in nude mice. The full-length (wild-type) LTBR protein was also found to manifest similar transforming activity. These observations suggest that LTBR, which belongs to the tumor necrosis factor receptor superfamily of proteins, may contribute to human carcinogenesis.

Keywords: Lymphotoxin-β receptor; Pancreatic ductal carcinoma; Retrovirus; cDNA expression library; Oncogene

Pancreatic ductal carcinoma (PDC) originates from pancreatic ductal cells and remains one of the most intractable human malignancies [1,2]. Effective therapy for PDC is hampered by the absence of specific clinical symptoms. At the time of diagnosis, most affected individuals are no longer candidates for surgical resection, and, even in patients who do undergo such surgery, the 5-year survival rate is only 20–30% [2].

The molecular pathogenesis of PDC has been the subject of intensive investigation. The gene *KRAS2* is frequently mutated and activated in PDC cells [3], and various tumor suppressor genes, including those for p53, p16, and BRCA2, are inactivated [4]. Furthermore, genetic or epigenetic alterations of genes important in apoptosis or in tumor cell invasion or metastasis have been detected in PDC cells [5]. However, mutations in *KRAS2* have also been identified in pancreatic tissue affected by nonmalignant chronic pancreatitis [6], and genetic changes truly specific to PDC remain to be uncovered. Improvement in the prognosis of individuals with PDC will require identification of the genetic or epigenetic alterations responsible for the aggressive nature of this cancer.

The focus formation assay with 3T3 or RAT1 fibroblasts has been extensively used to screen for transforming genes in various carcinomas [7]. Given that the expression of exogenous genes in this assay is usually controlled by their own promoters or enhancers, however, oncogenes are able to exert their transforming effects in the recipient cells only if these regulatory regions are active in fibroblasts, which is not always the case. Regulation of the transcription of test cDNAs by a promoter known to function efficiently in fibroblasts would be expected to

* Corresponding author. Fax: +81 285 44 7322.
E-mail address: hmano@jichi.ac.jp (H. Mano).

0006-291X/$ - see front matter © 2005 Elsevier Inc. All rights reserved.
doi:10.1016/j.bbrc.2005.10.080

ensure sufficient expression of the encoded protein in the focus formation assay. We have therefore now constructed a retroviral cDNA expression library from a human PDC cell line, MiaPaCa-2, and tested this library in the focus formation assay with 3T3 cells. For library construction, we took advantage of a polymerase chain reaction (PCR) system that preferentially amplifies full-length cDNAs. The resulting library had sufficient complexity with a high percentage of full-length cDNAs. With this library, we have revealed that the lymphotoxin-β receptor (LTBR) gene possesses transforming activity.

Materials and methods

Cell lines and culture. MiaPaCa-2, NIH 3T3, and BOSC23 cell lines were obtained from American Type Culture Collection and maintained in Dulbecco's modified Eagle's medium (DMEM)–F12 (Invitrogen, Carlsbad, CA) supplemented with 10% fetal bovine serum (Invitrogen) and 2 mM L-glutamine.

Construction of retroviral cDNA expression library. Total RNA extracted from MiaPaCa-2 cells with the use of an RNeasy Mini column and RNase-free DNase (Qiagen, Valencia, CA) was subjected to first-strand cDNA synthesis with PowerScript reverse transcriptase, SMART IIA oligonucleotide, and CDS primer IIA (Clontech, Palo Alto, CA). The resulting cDNAs were amplified for 14 cycles with 5′ PCR primer IIA and a SMART PCR cDNA synthesis kit (Clontech), with the exception that LA *Taq* polymerase (Takara Bio, Shiga, Japan) was substituted for the Advantage 2 DNA polymerase provided with the kit. The amplified cDNAs were treated with proteinase K, rendered blunt-ended with T4 DNA polymerase, and ligated to the BstXI-adaptor (Invitrogen). Unbound adaptors were removed with the use of a cDNA size-fractionation column (Invitrogen), and the remaining cDNAs were ligated into the BstXI site of the pMXS retroviral plasmid (kindly provided by T. Kitamura, Institute of Medical Science, University of Tokyo). The resulting pMXS-cDNA plasmids were introduced into ElecroMax DH10B cells (Invitrogen) by electroporation.

Focus formation assay. BOSC23 cells (1.8×10^6) were seeded into a 6-cm culture dish, cultured for 24 h, and then transfected with 2 μg of retroviral plasmids mixed with 0.5 μg of pGP plasmid (Takara Bio), 0.5 μg of pE-eco plasmid (Takara Bio), and 18 μl of Lipofectamine reagent (Invitrogen). Two days after transfection, polybrene (Sigma, St. Louis, MO) was added to the culture supernatant at a concentration of 4 μg/ml, and the supernatant was subsequently used to infect 3T3 cells for 48 h. The culture medium of the 3T3 cells was then changed to DMEM-F12 supplemented with 5% calf serum and 2 mM L-glutamine, and the cells were cultured for 2 weeks.

Recovery of cDNAs from transformants. Transformed 3T3 cell clones were harvested with a cloning syringe and cultured independently in 10-cm culture dishes. Genomic DNA was extracted from each clone by standard procedures and then subjected to PCR with 5′ PCR primer IIA and LA *Taq* polymerase for 50 cycles of 98 °C for 20 s and 68 °C for 6 min. Amplified DNA fragments were purified by gel electrophoresis and ligated into the pT7Blue-2 vector (EMD Biosciences, San Diego, CA) for nucleotide sequencing.

Anchorage-independent growth in soft agar. 3T3 cells (2×10^6) were infected with a retrovirus encoding a truncated form of LTBR or activated KRAS2 (see Results), resuspended in the culture medium supplemented with 0.4% agar [SeaPlaque GTG agarose (Cambrex, East Rutherford, NJ)], and seeded onto a base layer of complete medium supplemented with 0.5% agar. Cell growth was assessed after culture for 2 weeks.

Tumorigenicity assay in nude mice. 3T3 cells (2×10^6) infected with a retrovirus either encoding the truncated form of LTBR or containing the human wild-type LTBR cDNA (GeneCopoeia, Germantown, MD) were resuspended in 500 μl of phosphate-buffered saline and injected into each shoulder of a nu/nu Balb-c mouse (6-weeks old). Tumor formation was assessed after 3 weeks.

5′-Rapid amplification of cDNA ends (RACE). 5′-RACE was performed as described [8]. In brief, total RNA extracted from MiaPaCa-2 cells was used to generate cDNAs with an LTBR-specific primer (5′-GCAGTGGCTGTACCAAGTCA-3′). Excess primer was removed with a microconcentrator (Amicon, Austin, TX), and a poly(A) tail was added to the cDNAs by incubation with dATP and terminal deoxynucleotidyl-transferase (Invitrogen). The first PCR was performed with the dT-adaptor primer (5′-GACTCGAGTCGACATCGATTTTTTTTTTTTT TTTT-3′) and RACE-1 antisense primer (5′-CTCCCAGCTTCCAGCT ACAG-3′), and the second PCR with the adaptor primer (5′-GACTCGA GTCGACATCG-3) and RACE-2 antisense primer (5′-GAGCAGAAA GAAGGCCAGTG-3′). The amplification protocol for the first PCR comprised incubation at 94 °C for 2 min followed by 20 cycles of 94 °C for 1 min, 55 °C for 1 min, and 72 °C for 3 min. That for the second PCR included incubation at 94 °C for 2 min followed by 30 cycles of 94 °C for 1 min, 53 °C for 1 min, and 72 °C for 3 min.The final PCR products were ligated into pT7Blue-2 for nucleotide sequencing.

Results

Screening for transforming genes by focus formation assay

To screen for transforming genes in PDC, we constructed a cDNA expression library from MiaPaCa-2 cells. Full-length cDNAs were selectively amplified by a PCR protocol from total RNA isolated from the cells and were ligated into the retroviral vector pMXS. We obtained a total of 1.2×10^6 colony-forming units of independent library clones, from which we randomly selected 30 clones and examined the incorporated cDNAs. An insert of $\geqslant 500$ bp was present in 24 (80%) of the 30 clones and the average size of these 24 inserts was 1.84 kbp.

Introduction of the library plasmids into a packaging cell line yielded a recombinant retroviral library that was used to infect mouse NIH 3T3 fibroblasts. After culture of the infected cells for 2 weeks, a total of 18 transformed foci were identified. No foci were observed for 3T3 cells infected with the empty virus. Each transformed focus was isolated, expanded, and used to prepare genomic DNA. PCR amplification of the inserts identified a total of 29 cDNA fragments, each of which was ligated into a cloning vector and subjected to nucleotide sequencing from both ends. Screening of the 29 cDNA sequences against the public nucleotide sequence databases revealed that they showed >95% sequence identity to 13 independent genes, 11 known and 2 unknown (Table 1).

To confirm the transforming ability of the isolated cDNAs, we again ligated them into pMXS and used the corresponding retroviral vectors to re-infect 3T3 cells. Two of the 13 independent genes (clone ID #4, corresponding to *LTBR* [GenBank Accession No. NM_002342]; clone ID #10, corresponding to *KRAS2* [GenBank Accession No. NM_004985]) reproducibly induced the formation of transformed foci in 3T3 cells (Fig. 1). Further sequencing our *KRAS2* cDNA revealed that it has a point mutation leading to the amino acid change from a glycine residue at position 12 to a cysteine (data not shown). Whereas the oncogenic potential of mutated *KRAS2* has been

Table 1
MiaPaCa-2 cell cDNAs isolated from 3T3 transformants

Clone ID #	Gene symbol	GenBank No.	Presence of entire ORF
1	CGI-152	NM_020410	Yes
2	RAB28	NM_004249	Yes
3	MRPL43	NM_032112	Yes
4	LTBR	NM_002342	No
5	UBQLN1	NM_013438	Yes
6	TBC1D2	NM_018421	Yes
7	FKBP10	NM_021939	Yes
8	HCCA2	NM_053005	Yes
9	Unknown	AK123415	ND
10	KRAS2	NM_004985	Yes
11	STK11IP	NM_052902	Yes
12	Unknown	AA627562	ND
13	PFKP	NM_002627	Yes

ORF, open reading frame; ND, not determined.

extensively investigated [3], little is known of such activity for *LTBR*. We thus focused on *LTBR* for further analysis.

Identification of a truncated form of LTBR

Although the nucleotide sequence of both ends of our LTBR cDNA was identical to that of human *LTBR*, the size of our cDNA (1452 bp) was smaller than that (2136 bp) of the full-length cDNA previously described. We thus determined the complete nucleotide sequence of our cDNA, revealing that it starts at nucleotide position 685 of the reported sequence (NM_002342). The longest open reading frame in our cDNA begins at amino acid position 221 and ends at position 435 of the previously described LTBR protein; it therefore encodes a predicted protein of 215 amino acids with a calculated molecular mass of 22,692 Da (Fig. 2). Given that the nucleotide sequence surrounding the putative translation start site of our cDNA matches the consensus Kozak motif, the corresponding mRNA likely produces this NH_2-terminally truncated form of LTBR, which is hereafter referred to as short-type LTBR.

5′-RACE analysis of LTBR mRNA

To confirm the presence of an mRNA encoding short-type LTBR in MiaPaCa-2 cells, we performed 5′-RACE to determine the 5′ ends of LTBR mRNAs. The first strand of LTBR cDNAs was generated with an LTBR-specific reverse transcription (RT) primer (Fig. 2) from RNA isolated from MiaPaCa-2 cells. Poly(A) was added to the 3′ end of the cDNAs, which were then subjected to nested PCR in order to amplify the 5′ ends. PCR products (ranging from a few hundred to 2000 bp) were detected only when reverse transcriptase was included in the procedure (Fig. 3A), indicating that the products were synthesized from cDNA, not from genomic DNA. The nucleotide sequence of 96 randomly chosen PCR products was determined. Sixty-eight of the 96 products matched the LTBR cDNA sequence and the positions of their 5′ ends are indicated in Fig. 3B. Transcription of most of the mRNAs corresponding to these PCR products was initiated in the region immediately upstream of the translation start site for short-type LTBR, indicating the existence of multiple mRNAs for this truncated protein in vivo.

Confirmation of transforming activity of short-type LTBR

To confirm the transforming activity of short-type LTBR, we examined its effect on anchorage-independent growth of 3T3 cells in soft agar. Whereas cells infected with an empty virus did not grow in soft agar, those infected with a virus encoding short-type LTBR formed multiple foci in repeated experiments (Fig. 4A). In addition, 3T3 cells expressing activated *KRAS2* readily grew in the agar.

We also injected the infected cells into nude mice. Tumors formed at all ($n = 10$) sites injected with 3T3 cells expressing short-type LTBR (Fig. 4B). Again, 3T3 cells expressing activated *KRAS2* also generated tumors at a high frequency, whereas those infected with the empty virus did not induce tumor formation. Together, these results thus confirmed that short-type LTBR possesses transforming activity.

Transforming activity of wild-type LTBR

To determine whether the full-length (435-amino acid) LTBR protein also possesses oncogenic potential, we performed the focus formation assay and in vivo tumorigenicity assay with a recombinant retrovirus encoding the wild-type

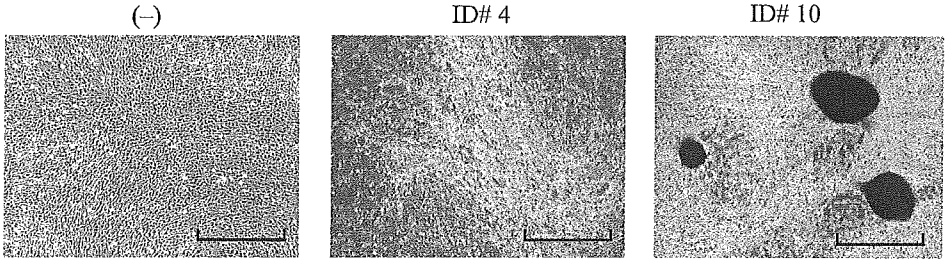

Fig. 1. Identification of transforming genes of MiaPaCa-2 cells. Mouse 3T3 cells were infected with an empty retrovirus (–) or with recombinant retroviruses harboring cDNAs corresponding to library clones ID #4 (short-type LTBR) or ID #10 (KRAS2). The cells were photographed after culture for 2 weeks. Scale bars, 1 mm.

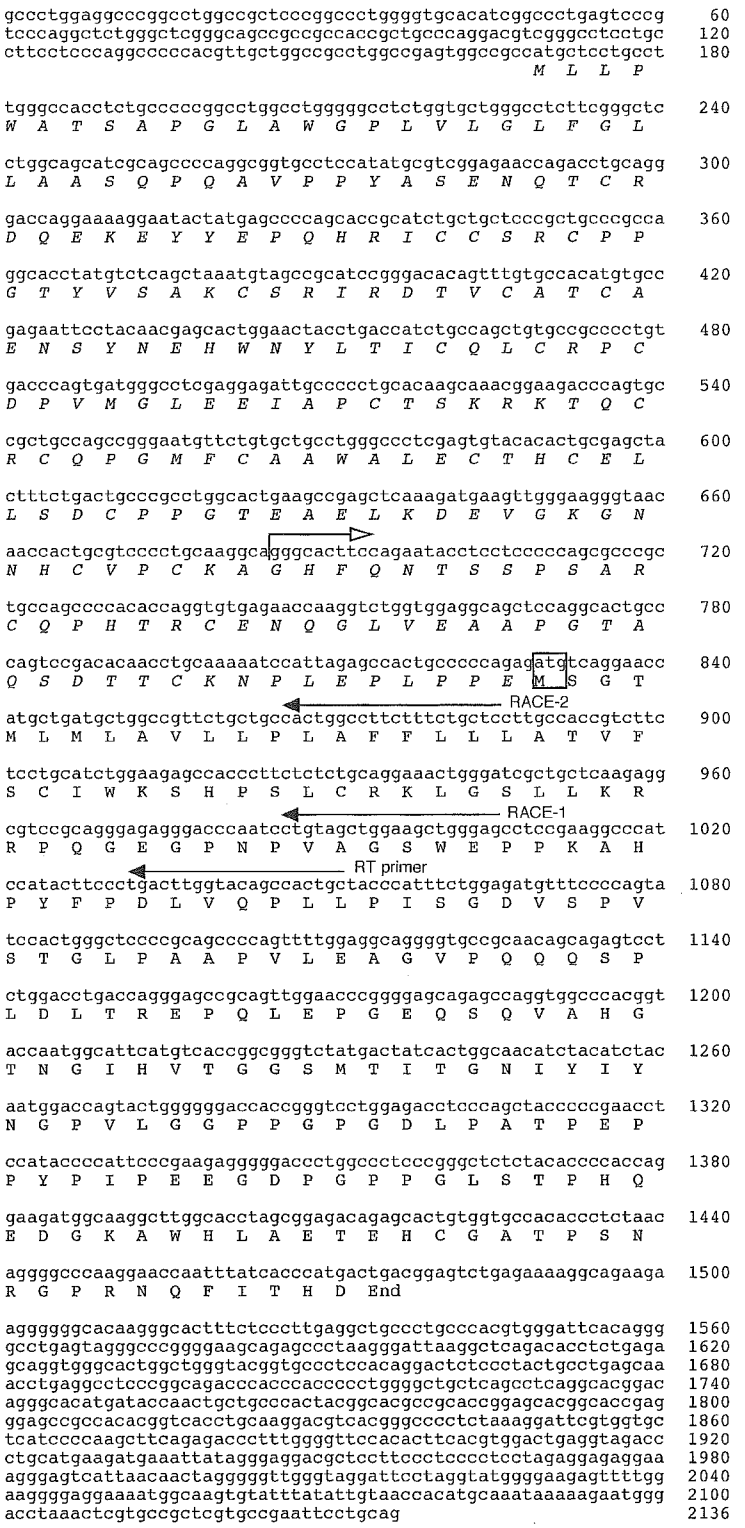

Fig. 2. Characterization of an LTBR cDNA isolated by screening for transformation activity. Amino acid residues of the full-length LTBR protein are aligned with the previously determined nucleotide sequence of LTBR cDNA (NM_002342). The cDNA isolated in the present study begins at nucleotide position 685 (open arrow) of the reported cDNA. The putative translation start site for the truncated (short-type) LTBR protein is boxed. The positions of primers used for 5′-RACE are indicated by closed arrows.

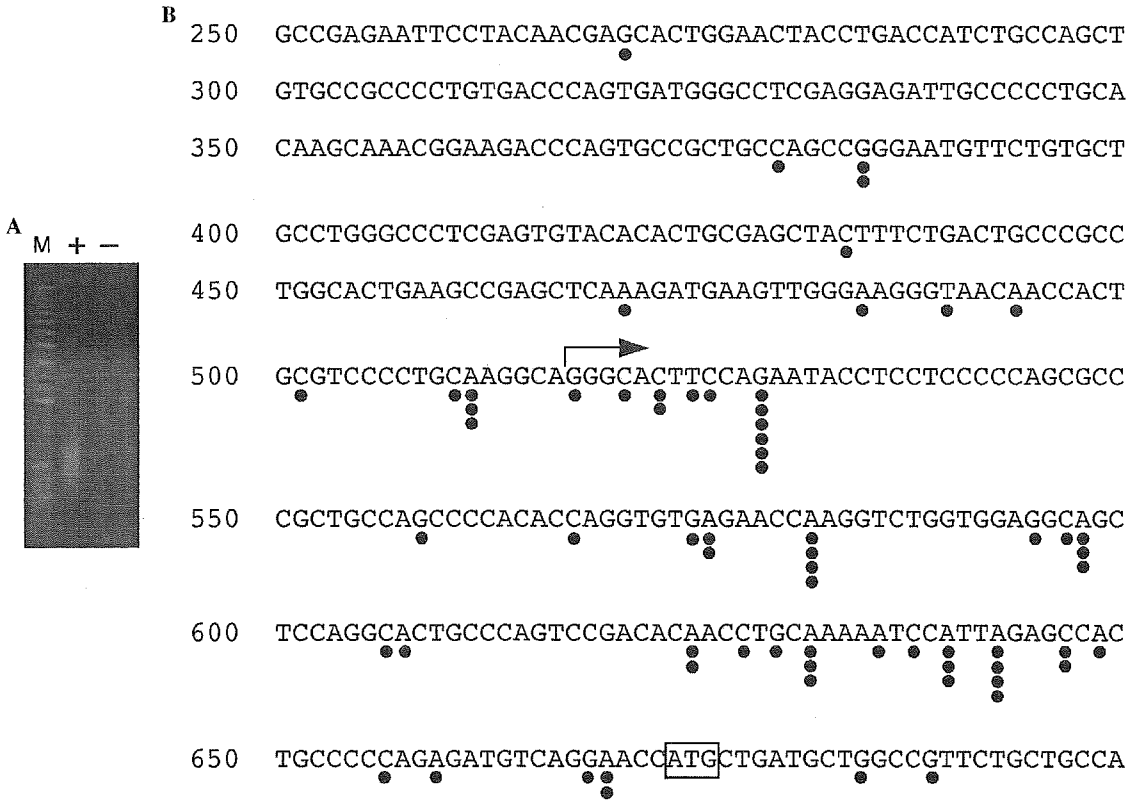

Fig. 3. 5′-RACE analysis of LTBR cDNA. (A) Total RNA of MiaPaCa-2 cells was incubated with the LTBR-specific RT primer in the presence (+) or absence (−) of reverse transcriptase, and resulting cDNA was subjected to PCR-based 5′-RACE. The PCR products were fractionated by electrophoresis through a 1.8% agarose gel and stained with ethidium bromide. Lane M, 1-kb DNA ladder. (**B**) The positions of the 5′ ends of 5′-RACE products are indicated by closed circles in alignment with the reported LTBR cDNA sequence. Numbers on the left indicate nucleotide positions relative to the translation initiation site of the full-length (wild-type) cDNA. The arrow indicates the 5′ end of the cDNA isolated by retroviral screening in the present study; the putative translation start codon of this cDNA is boxed.

human protein. The infected cells generated both transformed foci in vitro and tumors in nude mice (Fig. 5).

Discussion

In the present study, we constructed a retroviral cDNA expression library for a PDC cell line. Given that 80% (24/30) of the viral plasmids contained cDNA inserts and that the overall clone number was >1 million, this library should represent most of the mRNAs in MiaPaCa-2 cells. We infected 3T3 mouse fibroblasts with this recombinant library to screen for transforming genes with a focus formation assay. This screen identified *KRAS2* with an activating mutation as a transforming gene of MiaPaCa-2 cells, supporting the fidelity of our approach.

Our screen also identified a transforming cDNA that encodes an NH_2-terminally truncated form of LTBR. 5′-RACE analysis revealed the existence of mRNAs for this short-type LTBR in MiaPaCa-2 cells, and retrovirus-mediated expression of the isolated cDNA in 3T3 cells conferred the ability to grow in soft agar in vitro as well as the ability to form tumors in vivo.

LTBR belongs to the tumor necrosis factor (TNF) receptor superfamily [9] and binds two functional ligands, lymphotoxin-α1β2 and LIGHT [10,11]. LTBR is expressed by many cell types (but not by lymphocytes), whereas expression of the LTBR ligands is restricted to activated lymphocytes [11]. Signaling by LTBR is important in the development of lymphoid tissue and in generation of adaptive humoral immune responses [12,13]. In general, LTBR function is thought to be linked to apoptosis. Indeed, activation of LTBR by its endogenous ligands or by anti-receptor antibodies triggers the death of various tumor cell lines [14,15]. Activation of the LIGHT-LTBR signaling pathway in tumor cells also induces marked chemokine-dependent recruitment of T cells to tumors, resulting in the rejection of established tumor cells [16].

LTBR activation has also been linked to tumor development, however. Its activation in fibrosarcoma cells thus induces angiogenesis and tumor growth by triggering the release of macrophage inflammatory protein-2, an angiogenic CXC chemokine [17]. Although oncogenic potential has not previously been demonstrated for LTBR, our data now show that both the full-length and truncated forms of this protein possess transforming activity even in the absence of exogenous cognate ligands. A high level of expression of LTBR conferred by the retroviral long terminal repeat in our experiments might have resulted in self-oligomerization

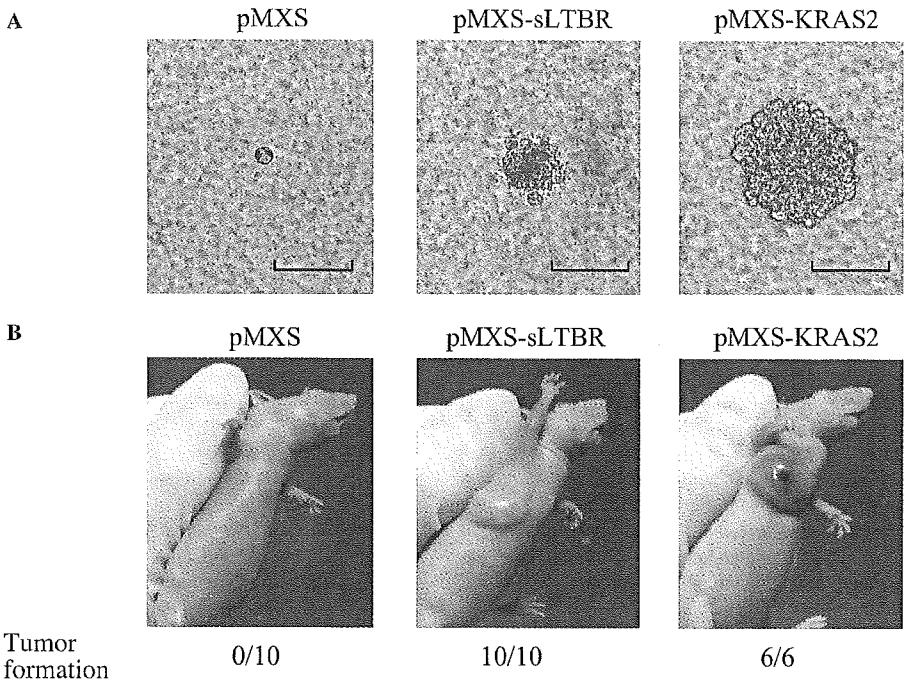

Fig. 4. Transforming activity of short-type LTBR. (A) Focus formation assay. 3T3 cells infected either with empty retrovirus (pMXS) or with retroviruses encoding short-type LTBR (pMXS-sLTBR) or activated KRAS2 (pMXS-KRAS2) were seeded into soft agar and incubated for 2 weeks. Scale bars, 100 μm. (B) Tumorigenicity assay. Cells infected as in (A) were injected into the shoulder of nude mice and tumor formation was examined after 3 weeks. The frequency of tumor formation determined is indicated.

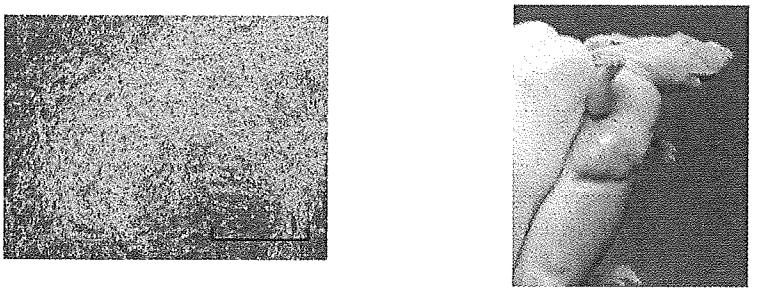

Fig. 5. Transforming activity of full-length LTBR. The transforming activity of a retroviral vector encoding full-length (wild-type) LTBR was evaluated by the focus formation assay (left) or the in vivo tumorigenicity assay (right). Scale bar, 1 mm.

of the protein. It is thus likely that LTBR exerts its oncogenic function in a tissue- and context-dependent manner. As shown here for PDC, it will be important to determine whether LTBR also contributes to the mechanism of transformation in other human malignancies.

Acknowledgments

This work was supported in part by a grant for Third-Term Comprehensive Control Research for Cancer from the Ministry of Health, Labor, and Welfare of Japan as well as by a grant for "High-Tech Research Center" Project for Private Universities: Matching Fund Subsidy (2002–2006) from the Ministry of Education, Culture, Sports, Science and Technology of Japan.

References

[1] S. Rosewicz, B. Wiedenmann, Pancreatic carcinoma, Lancet 349 (1997) 485–489.
[2] P.C. Bornman, I.J. Beckingham, Pancreatic tumours, Br. Med. J. 322 (2001) 721–723.
[3] M. Tada, M. Omata, M. Ohto, Clinical application of ras gene mutation for diagnosis of pancreatic adenocarcinoma, Gastroenterology 100 (1991) 233–238.
[4] S.R. Bramhall, The use of molecular technology in the differentiation of pancreatic cancer and chronic pancreatitis, Int. J. Pancreatol. 23 (1998) 83–100.

[5] G. Schneider, J.T. Siveke, F. Eckel, R.M. Schmid, Pancreatic cancer: basic and clinical aspects, Gastroenterology 128 (2005) 1606–1625.
[6] A. Yanagisawa, K. Ohtake, K. Ohashi, M. Hori, T. Kitagawa, H. Sugano, Y. Kato, Frequent c-Ki-ras oncogene activation in mucous cell hyperplasias of pancreas suffering from chronic inflammation, Cancer Res. 53 (1993) 953–956.
[7] S.A. Aaronson, Growth factors and cancer, Science 254 (1991) 1146–1153.
[8] M.A. Frohman, M.K. Dush, G.R. Martin, Rapid production of full-length cDNAs from rare transcripts: amplification using a single gene-specific oligonucleotide primer, Proc. Natl. Acad. Sci. USA 85 (1988) 8998–9002.
[9] P.D. Crowe, T.L. VanArsdale, B.N. Walter, C.F. Ware, C. Hession, B. Ehrenfels, J.L. Browning, W.S. Din, R.G. Goodwin, C.A. Smith, A lymphotoxin-β-specific receptor, Science 264 (1994) 707–710.
[10] J.L. Browning, I.D. Sizing, P. Lawton, P.R. Bourdon, P.D. Rennert, G.R. Majeau, C.M. Ambrose, C. Hession, K. Miatkowski, D.A. Griffiths, A. Ngam-ek, W. Meier, C.D. Benjamin, P.S. Hochman, Characterization of lymphotoxin-αβ complexes on the surface of mouse lymphocytes, J. Immunol. 159 (1997) 3288–3298.
[11] W.R. Force, B.N. Walter, C. Hession, R. Tizard, C.A. Kozak, J.L. Browning, C.F. Ware, Mouse lymphotoxin-β receptor. Molecular genetics, ligand binding, and expression, J. Immunol. 155 (1995) 5280–5288.
[12] A. Futterer, K. Mink, A. Luz, M.H. Kosco-Vilbois, K. Pfeffer, The lymphotoxin β receptor controls organogenesis and affinity maturation in peripheral lymphoid tissues, Immunity 9 (1998) 59–70.
[13] R.M. Locksley, N. Killeen, M.J. Lenardo, The TNF and TNF receptor superfamilies: integrating mammalian biology, Cell 104 (2001) 487–501.
[14] J.L. Browning, K. Miatkowski, I. Sizing, D. Griffiths, M. Zafari, C.D. Benjamin, W. Meier, F. Mackay, Signaling through the lymphotoxin β receptor induces the death of some adenocarcinoma tumor lines, J. Exp. Med. 183 (1996) 867–878.
[15] I.A. Rooney, K.D. Butrovich, A.A. Glass, S. Borboroglu, C.A. Benedict, J.C. Whitbeck, G.H. Cohen, R.J. Eisenberg, C.F. Ware, The lymphotoxin-β receptor is necessary and sufficient for LIGHT-mediated apoptosis of tumor cells, J. Biol. Chem. 275 (2000) 14307–14315.
[16] P. Yu, Y. Lee, W. Liu, R.K. Chin, J. Wang, Y. Wang, A. Schietinger, M. Philip, H. Schreiber, Y.X. Fu, Priming of naive T cells inside tumors leads to eradication of established tumors, Nat. Immunol. 5 (2004) 141–149.
[17] T. Hehlgans, B. Stoelcker, P. Stopfer, P. Muller, G. Cernaianu, M. Guba, M. Steinbauer, S.A. Nedospasov, K. Pfeffer, D.N. Mannel, Lymphotoxin-β receptor immune interaction promotes tumor growth by inducing angiogenesis, Cancer Res. 62 (2002) 4034–4040.